

3D Face Morphing Attacks: Generation, Vulnerability and Detection

Jag Mohan Singh, *Member, IEEE*

Raghavendra Ramachandra, *Senior Member*

Abstract—Face Recognition systems (FRS) have been found vulnerable to morphing attacks, where the morphed face image is generated by blending the face images from contributory data subjects. This work presents a novel direction towards generating face morphing attacks in 3D. To this extent, we have introduced a novel approach based on blending the 3D face point clouds corresponding to the contributory data subjects. The proposed method will generate the 3D face morphing by projecting the input 3D face point clouds to depth-maps & 2D color images followed by the image blending and wrapping operations performed independently on the color images and depth maps. We then back-project the 2D morphing color-map and the depth-map to the point cloud using the canonical (fixed) view. Given that the generated 3D face morphing models will result in the holes due to a single canonical view, we have proposed a new algorithm for hole filling that will result in a high-quality 3D face morphing model. Extensive experiments are carried out on the newly generated 3D face dataset comprised of 675 3D scans corresponding to 41 unique data subjects. Experiments are performed to benchmark the vulnerability of automatic 2D and 3D FRS and human observer analysis. We also present the quantitative assessment of the quality of the generated 3D face morphing models using eight different quality metrics. Finally, we have proposed three different 3D face Morphing Attack Detection (3D-MAD) algorithms to benchmark the performance of the 3D MAD algorithms.

Index Terms—Biometrics, Face Recognition, Vulnerability, 3D Morphing, Point Clouds, Image Morphing, Morphing Attack Detection

I. INTRODUCTION

Face Recognition Systems (FRS) are being widely deployed in numerous applications related to security settings such as automated border control (ABC) gates and commercial settings like eCommerce and e-banking scenarios. The rapid evolution of the FRS can be attributed to the advances in deep learning FRS [1], [2] which provided improved accuracy in real-world and uncontrolled scenarios. These factors accelerated the use of 2D face images in the electronic Machine Readable Document (eMRTD), which is exclusively used to verify the passport's owner at the various ID services, including border control (both automatic and human). Since most of the countries still use the printed passport images for the passport application process, the face morphing attack has indicated the vulnerability on both human and automatic FRS [3], [4]. Face morphing is the process of blending the multiple face images either based on the facial landmarks [5] or based on the Generative Adversarial Networks [6] to generate the morphing face image. The extensive

analysis reported in literature [7]–[10] has demonstrated the vulnerability of the 2D face morphing images to both deep learning and commercial-off-the-shelf FRS.

There exist several techniques to detect the 2D face morphing attacks that can be classified as [11] (a) Single image-based Morph Attack Detection (S-MAD): where the face Morphing Attack Detection (MAD) techniques will use the single face image to arrive at the final decision (b) Differential Morphing Attack Detection (D-MAD): where a pair of 2D face images are used to arrive at the final decision. Both S-MAD and D-MAD techniques are extensively studied in the literature that has resulted in several MAD techniques. The reader is advised to refer to the recent survey by Venkatesh et al. [11] to get a comprehensive overview of the existing 2D MAD techniques. Despite the rapid progress in 2D MAD techniques, the recent evaluation report from NIST FRVT MORPH [12] indicates the degraded detection of 2D face morphing attacks. Thus, the 2D MAD attacks, especially in the S-MAD scenario, show significant challenges for reliable detection. These factors motivate us to explore 3D face morphing so that the use of depth information may provide a reliable cue that makes the morphing detection easier.

The 3D face recognition is widely studied from past several decades that has resulted in the several real-life security-based applications with 3D face photo-based national ID cards [13], [14], [15], 3D face photo-based driving license card [15] and 3D face-based automatic border control gates (ABC) [16]. The real case reported in [17] has demonstrated the use of a 2D rendered face image from a 3D face model instead of a real 2D face photo to obtain the ID card bypassing the human observers at the ID card issuing protocol. Although most real-life 3D face applications are based on comparing the 3D face models against 2D face images for verification, this is mainly because epassport uses a 2D face image.

However, the use of 3D to 3D comparison will be realistic, especially in the border control scenario as both ICAO 9303 [18], and ISO/IEC 19794-5 [19] standards are well defined to accommodate the 3D face model in the 3rd generation epassport. The 3D face ID cards are a reality as they are being deployed in the countries like UAE [13] that can facilitate both human observers and automatic FRS to achieve accurate, secure, and reliable ID verification. Further, the evolving technology has made it possible for 3D face imaging on handheld and smartphones (e.g., Apple Face ID [20] uses 3D face recognition) that can further enable remote ID verification based on the 3D face verification. These factors have further motivated us to investigate the feasibility of generating the 3D face morphing and study their vulnerability and detection.

Norwegian University of Science and Technology (NTNU), Norway
e-mail: (jag.m.singh@ntnu.no; raghavendra.ramachandra@ntnu.no).

Both authors have equally contributed for this work.

In this work, we present a novel method for generating 3D face morphing using 3D point clouds. Given the 3D scans from the accomplished and the malicious actors, the proposed method will project the 3D point clouds to the depth-maps & the 2D color images, which are independently blended, warped and back-projected to the 3D to obtain the 3D face morphing. This is the first work addressing 3D face morphing generation and detection to the best of our knowledge. More particularly, we aim to seek answers to the following research questions, which will be answered systematically in this paper:

- **RQ#1:** Does the proposed 3D face morphing generation technique yield a high-quality 3D morphed model?
- **RQ#2:** Does the generated 3D face morphing model indicate the vulnerability for both automatic 3D FRS and human observers?
- **RQ#3:** Are the generated 3D face morphing models more vulnerable when compared to 2D face morphing images for both automatic 3D FRS and human observers?
- **RQ#4:** Does the 3D point cloud information be used to detect the 3D face morphing attacks reliably?

We systematically address these research questions through our contributions listed as follows:

- We present a novel 3D face morphing generation method based on the point clouds obtained by fusion of depth maps and 2D color images to generate the 3D face morphing model.
- Extensive analysis of the vulnerability of the generated 3D face morphing is studied by quantifying the attack success rate to 3D FRS. The vulnerability analysis is also performed using 2D FRS (both deep learning and COTS).
- Human observer analysis for detecting the 3D face morphing and 2D face morphing is presented to study the significance of depth information in detecting the morphing attack.
- The quantitative analysis of the generated 3D morphed face models is presented using eight quality features representing both color and geometry.
- We present three different 3D MAD techniques based on the deep features from point clouds to benchmark the 3D face MAD.
- A new 3D face dataset with bona fide and morphed models are developed corresponding to 41 unique data subjects. The whole dataset had 675 3D scans. We collected a new 3D face dataset as we were interested in capturing high-resolution (suitable for ID enrolment) inner face data [21] Our 3D face dataset consists of raw 3D scans (number of 3D vertices between 31289 & 201065) and processed 3D scans (number of 3D vertices between 35950 & 121088), which is much higher than existing 3D face datasets¹.

In the rest of the paper we introduce the proposed method in Section II and experiments & results in Section III. This is followed by discussion about the different aspects of the proposed method in Section IV, followed by limitations &

potential future-works in Section V and finally conclusions in Section VI.

II. PROPOSED METHOD

Figure 1 shows the block diagram of the proposed 3D face morphing generation framework based on the 3D point clouds. We are motivated to employ the 3D point clouds over traditional 3D triangle mesh for two main reasons. The first is that connectivity information in a 3D triangle mesh leads to overhead storage, processing, managing, and manipulating the triangular meshes. Thus, the use of 3D triangle meshes will significantly increase both compute and memory, making it less suitable for low-compute devices. The second reason is that the commodity scanning devices (for example, the Artec Sensor) can reproduce detailed colored point clouds that capture both appearance and geometry. Thus, allowing us to generate high-quality 3D face morphing attacks.

However, the 3D face morphing generation using point clouds introduces numerous challenges (a) Establishing a dense 3D correspondence between two different bona fide 3D point clouds that are to be morphed. Because 3D face point clouds from two different subjects are affected by various factors such as difference in input point density, reliable detection of 3D facial key-points, and estimation of affine/perspective warping (b) Locally affine deformation present between two different 3D point clouds to be morphed is difficult to estimate [22]–[24]. (c) The misalignment of dense 3D correspondence between the two different 3D point clouds to be morphed increases with non-rigid deformation [25]. To effectively address these challenges, the proposed method consists of four stages, including (1) point cloud reconstruction and cleanup, (2) 3D morph generation, (3) hole-filling algorithm, and (4) final cleanup. In the following subsections, these steps are discussed in detail.

A. Point Cloud Reconstruction & Cleanup

We capture a sequence of raw 3D scans using Artec Eva sensor [26] from two different data subjects that are to be morphed (S_1 and S_2). In this work, we consider the case of morphing two data subjects at a time because of its real-life applications, as demonstrated in several 2D face morphing works [3], [11]. We process both S_1 and S_2 by performing a series of pre-processing operations such as noise filtering, texturing, and fusion of input depth maps to generate the corresponding point clouds P_1 , and P_2 . These operations are carried out using Artec Eva Studio SDK filters together with the Meshlab filter [27]. The cleaned and process point clouds are qualitatively shown in Figure 1.

B. 3D Morph Generation Pipeline

In the next step, we process the point clouds P_1 , and P_2 to generate a 3D face morphing point cloud by following series of operations which are discussed below:

¹The reader is referred to Table 1 of 3D face datasets (inner face data only) from the survey by Egger et al. [21]

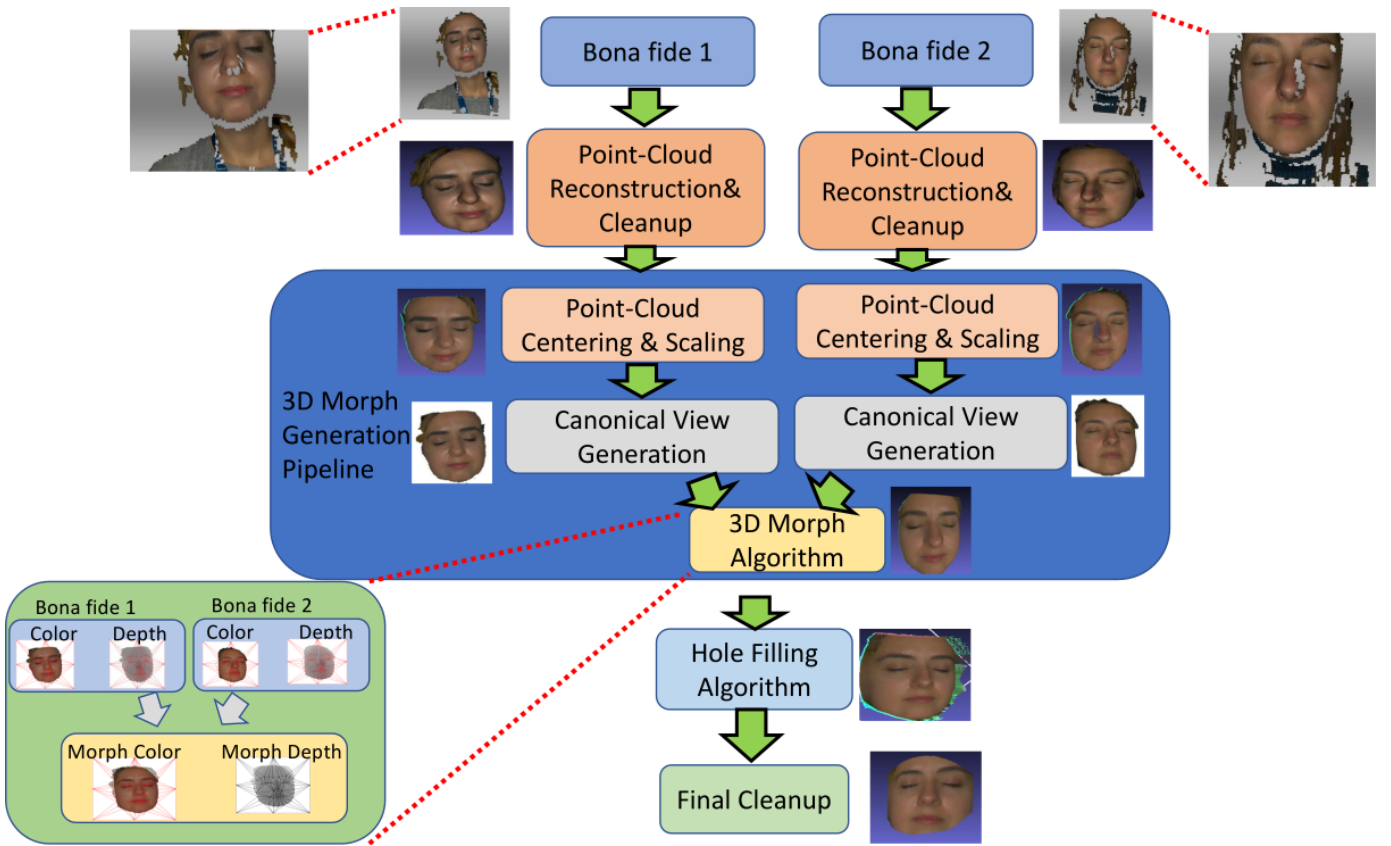


Fig. 1. Block diagram of the proposed 3D face morphing generation technique

1) **Point-Cloud Centering & Scaling:** We first compute the minimum enclosing spheres using the algorithm from Gärtner et al. [28] to get the two bounding spheres with centres and radii (C_1, r_1) , & (C_2, r_2) corresponding to the point cloud P_1 , and P_2 respectively. Note $P_1 = (v_1^1, \dots, v_1^{n1})$ where v_1^i is the i^{th} 3D vertex, and $n1$ is the number of points in the point cloud P_1 , and $P_2 = (v_2^1, \dots, v_2^{n2})$ where v_2^i is the i^{th} 3D vertex, and $n2$ is the number of points in the point cloud P_2 . We then subtract the sphere center C_1 from each 3D vertex of P_1 and we repeat the same operation on P_2 with C_2 . Finally, the centered point clouds are further scaled to the common radius which normalizes the 3D point clouds to the common scale. The resulting centered and scaled point clouds corresponding to P_1 and P_2 are denoted as PC_1 , and PC_2 , respectively. The qualitative result of this operation is as shown in the Figure 1 that shows centered and scaled 3D point clouds.

2) **Canonical View Generation:** This step performs the fine alignment by projecting the 3D face point clouds PC_1 and PC_2 to the canonical (fixed) view. This step aims to keep the view and projection matrix identical to the 3D face point clouds PC_1 and PC_2 . We then project PC_1 and PC_2 to generate 2D color images and depth maps using the canonical view parameters. The generated 2D color images and depth maps are denoted as (I_1, D_1) and (I_2, D_2) that corresponds to the point clouds PC_1 , and PC_2 respectively. We particularly choose the canonical view for the fine alignment because the traditional scheme of alignment such as Iterative Closest

Point (ICP) [25] doesn't provide a good alignment result when used on point clouds [23]. This can be attributed to the limitations of the ICP to function when a locally affine/non-rigid deformation exists between the point clouds [29] The qualitative results of the canonical view transformation are shown in Figure 1 which demonstrates the aligned 2D color images, and depth maps zoomed in the inset image.

3) **3D Morph Generation:** Given the 2D face color images (I_1, I_2) and depth-maps (D_1, D_2) corresponding to PC_1, PC_2 . We perform the morphing operation as explained in the Algorithm 1. The primary idea is to perform the morphing in 2D and back-project to 3D. The primary motivation of using a 2D morph generation method is to address the challenge of finding correspondence between PC_1 and PC_2 . The underlining idea is to perform the steps of morphing (facial landmark detection, Delaunay triangulation, & warping) on 2D color images and re-use the same (facial landmark locations, triangulation, and warping) on the depth maps. In this work, we have used the blending (morphing) factor (α) as 0.5 as it is well demonstrated to be highly vulnerable in the earlier works on 2D face morphing [6]. The morphing is carried out as mentioned in the equation below:

$$\begin{aligned}
 I_M &= \alpha * I_1(K'_1) + (1 - \alpha) * I_2(K'_2) \\
 K'_1 &= w_1^M(K_1) \\
 K'_2 &= w_2^M(K_2) \\
 K_M &= \alpha * K_1 + (1 - \alpha) * K_2
 \end{aligned} \tag{1}$$

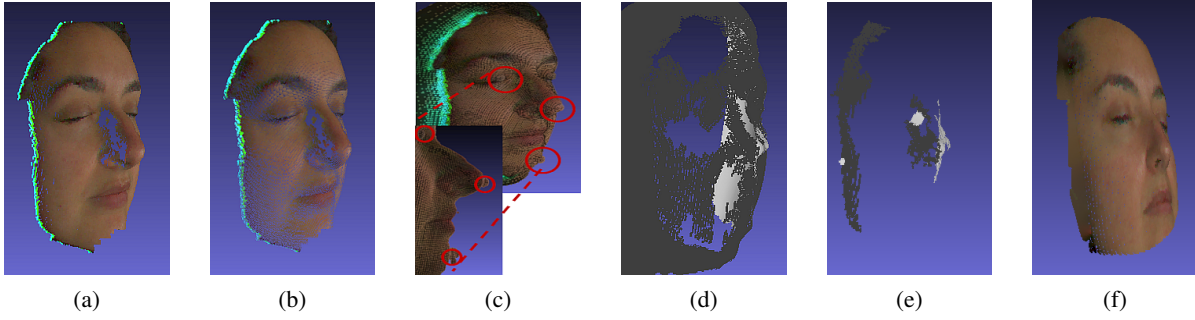


Fig. 2. Qualitative results of the hole filling algorithms (a) Input Point Cloud with holes, (b) Point Cloud with Normals which has noise, (c) Point Cloud with Screened Poisson Reconstruction [30] where artifacts are shown in the inset, (d) Point Cloud Reconstructed with APSS [31], (e) Point Cloud Reconstructed with RIMLS [32], (f) Point Cloud Hole Filled using Proposed Method

Algorithm 1 3D Face Morphing Algorithm

Input (I_1, I_2, D_1, D_2, CV)

Output (P_M)

- 1: Detect Facial Keypoints on K_1 on I_1 , and K_2 on I_2 using Dlib [33], and generate key-points of the morph using Equation 1.
 - 2: Perform Delaunay Triangulation on K_M which is obtained by blending K_1 and K_2 using Equation 1.
 - 3: Estimate Affine Warping between corresponding triangles of K_1 & K_M denoted as w_1^M , and for K_2 & K_M denoted as w_2^M .
 - 4: Apply affine warping w_1^M on I_1 to obtain I_{1M} , and on D_1 to obtain D_{1M} .
 - 5: Apply affine warping w_2^M on I_2 to obtain I_{2M} , and on D_2 to obtain D_{2M} .
 - 6: Obtain morphed color image I_M using the warped key-points from the color images I_1 , and I_2 using Equation 1, and morphed depth map D_M using Equation 2.
 - 7: Obtain the morphed point cloud by back-projecting I_M , and D_M to obtain the colored 3D point cloud P_M with 3D coordinates $\forall i \in \{1, \dots, n3\} (x_i, y_i, z_i) = (x_i, y_i, D_M(x_i, y_i))$ and color $\forall i \in \{1, \dots, n3\} \text{Color}(x_i, y_i, z_i) = C_M(x_i, y_i)$ where $n3 = \min(n1, n2)$.
-

where α is the blending factor, K_1 denotes 2D facial landmark locations corresponding to I_1 , K_2 denotes 2D facial landmark locations corresponding to I_2 , K_M is generated by blending K_1 , & K_2 , w_1^M denotes the warping function from K_1 to K_M , w_2^M denotes the warping function from K_2 to K_M , and I_M is the morphed 2D color image. Similarly, the same operations are carried out on the depth maps as shown in the equation below:

$$D_M = \alpha * D_1(K_1') + (1 - \alpha) * D_2(K_2') \quad (2)$$

where D_M is the morphed depth-map.

In the next step, we back-project I_M , and D_M to get the 3D face morphing point cloud $P_M = (v_M^1, \dots, v_M^{n3})$ where $n3 = \min(n1, n2)$ is the number of vertices. Note each 3D vertex is obtained using $i = 1^{n3}(x_i, y_i, z_i) = (x, y, D_M(x, y))$ and the qualitative results is shown in Figure 1. However, generating

the 3D face morphing will result in multiple holes due to a single canonical view. These holes are visible from the other views. Therefore, we present a novel hole-filling algorithm further to improve the perceptual visual quality of the 3D face morphing.

Algorithm 2 Hole Filling Point Cloud

Input ($n4$ -views)

Output (C_{hf}, D_{hf}, P_{hf})

- 1: Generate n pairs of color-maps, and depth-maps $\{(C_1, D_1), (C_2, D_2), \dots, (C_j, D_j), \dots, (C_{n4}, D_{n4})\}$, translated from the canonical view.
 - 2: **for** $j \leftarrow 1$ to $n4$ **do**
 - 3: Perform Image In-painting [34] on C_j , and D_j .
 - 4: Perform Image Registration of C_j with the canonical view-point color-map C_{CV} using the following steps:
 - 5: Feature Computation using Oriented FAST and Rotated BRIEF (ORB) Descriptor [35].
 - 6: Brute-Force Matching of features using Hamming Distance.
 - 7: Homography computation using inlier features.
 - 8: Perspectively warp the color-map, and the depth-map using computed homography.
 - 9: **end for**
 - 10: Average all the registered color-maps (C_{hf}) and the depth-maps (D_{hf}).
 - 11: Back-Project the averaged color-map and depth-map from 2D to 3D to generate hole-filled point cloud (P_{hf}) using the canonical view parameters.
-

C. Hole Filling Algorithm

In this step, we propose a new hole-filling algorithm tailored to this specific 3D face morphing generation problem. Since the holes are visible from different views, filling the holes in these views is necessary to improve the perceptual visual quality. Therefore, we transform the 3D face morphing point cloud P_M multiple times independently to generate P_M^j where $j = 1..n4$ and $n4$ is the number of transformations and

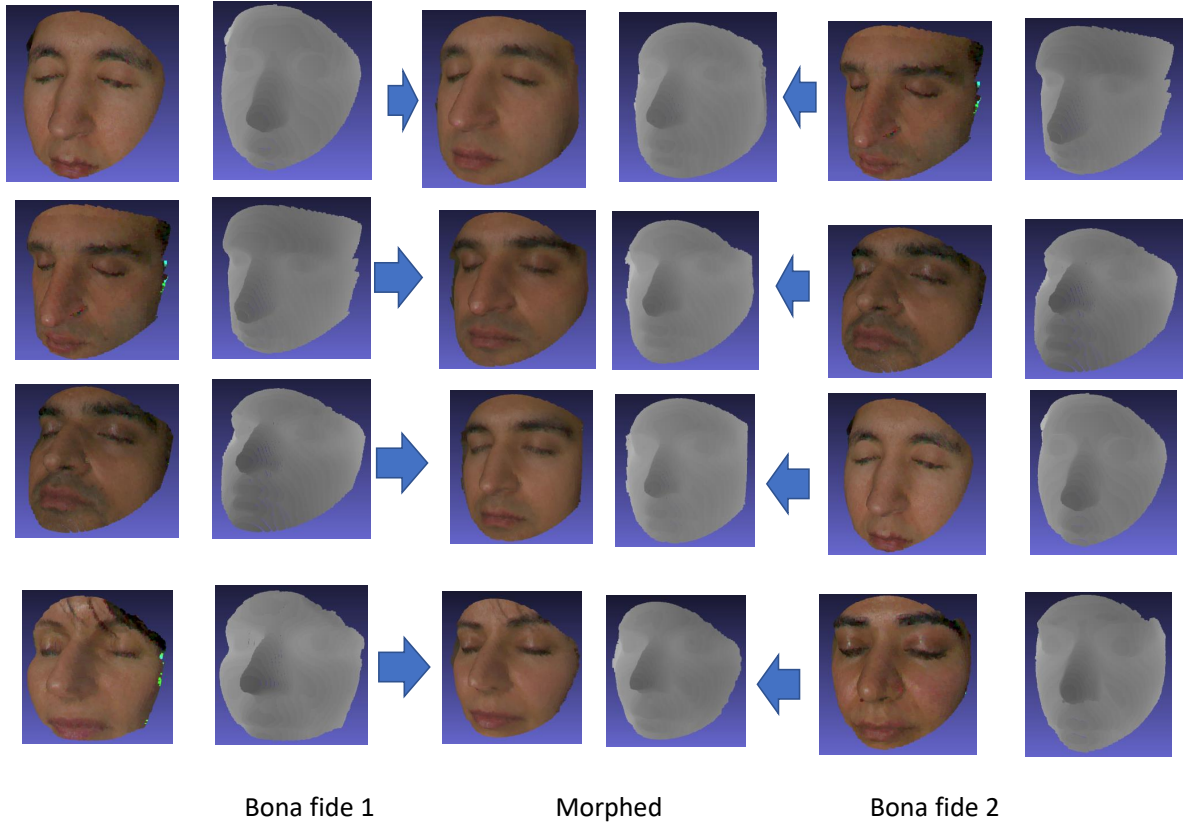


Fig. 3. Illustration of 2D color image and depth maps for bona fide and morphs generated using the proposed method

each transformation is a 3D translation [36]. In this work, we empirically choose the number of 3D translations to 7 to balance computational cost and the visual quality achieved after the hole filling. Using more 3D translations will significantly increase the computational cost and fail to improve the visual quality. In fact, we tried the conventional approach of hole filling using 3D triangulation of 3D point cloud proposed in [30], [31], [32]. Figure 2 shows the qualitative results of three different SOTA triangulation algorithms that indicate the non-satisfactory results. This is because 3D orientation (3D normal) estimation indicates artifacts in the 3D triangulated mesh. Therefore, filling holes directly in the 3D point cloud is challenging, as the underlying surface (manifold) is not known in advance. The errors in 3D orientation estimation make it difficult to employ the conventional 3D hole filling approaches.

This has motivated us to devise a new approach to achieve effective hole filling. To this extent, we project each point cloud P_M^j to the 2D face morphing color image (C_j) and its corresponding depth-map (D_j). We fill the holes in C_j & D_j using steps 2 to 9 described in Algorithm 2. Finally, we obtain the hole-filled 3D face morphing point cloud (P_{hr}) as indicated in steps 10 and 11 in Algorithm 2. Figure 2 (e) shows the qualitative results of the proposed hole filling that indicated the superior visual quality compared to the existing methods.

D. Final Cleanup Algorithm

The final cleanup is performed using a clipping region outside a portion of the bounding sphere. The final result from our proposed 3D face morphing, a point cloud, is shown in Figure 3 for a few data subjects².

III. EXPERIMENTS AND RESULTS

In this section, we present the discussion on extensive experiments carried out on the newly acquired 3D face dataset. We discuss the quantitative results of the various experiments, including vulnerability study on automatic FRS and human observer study, quantitative quality estimation based on color and geometry of the generated 3D face morphing models and automatic detection of 3D MAD attacks.

A. 3D Face Data Collection

In this work, we have constructed a new 3D face dataset using the Artec Eva 3D scanner [26]. The data collection is carried out in an indoor lighting environment. The data subjects are asked to sit on the chair by closing their eyes to avoid the light's strong reflection from the 3D scanner. The 3D scanner is moved in the vertical direction to capture the 3D sequence.

²Supporting Video is available at <https://folk.ntnu.no/jagms/SupportingVideo.mp4>

3D face Bona fide		
Total Data Subjects	Males	Females
41	28	13
Total 3D samples	Males	Females
330	224	106
3D face Morphs		
Total 3D Morphs	Males	Females
345	278	67

TABLE I
STATISTICS OF NEWLY COLLECTED 3D FACE DATASET

We have used the Artec Studio Professional 14 for the 3D data collection and processing. We have collected the 3D face data from 41 data subjects which include 28 males and 13 females. We have captured nine to ten samples for each data subject in three different sessions in three days. The statistics of the whole 3D face dataset are summarized in Table I.

One can argue that we might have used the existing 3D face datasets such as FRGC [37] and BU-3DFE [38]. However, the FRGC dataset provides a single depth map and a color image. Thus, a high-quality point cloud cannot be generated. Further, the dataset has a few misaligned color images and depth maps [39] that will result in a low-quality 3D morphing generation. The BU-3DFE [38] dataset does provide 3D models, but these are perfectly registered, and the capture conditions are identical for all the subjects. This does not model the real-world scenario of capturing 3D point clouds with changes in capture conditions that could happen during data collection. The quality of our 3D face dataset has a much higher number of 3D vertices between 35950 & 121088 for the inner face compared to previous methods [21]. These factors motivated us to generate a new 3D face dataset to enable a high-quality 3D face morphing generation suitable for the ID control scenario.

B. Human Observer Analysis

We perform the human observer analysis to evaluate the human detection performance of the generated 3D morphs. The survey is set up online³ and is created using PHP, & HTML-CSS tools. GDPR norms are followed during the survey creation, and participants' email (used only for registration to avoid duplication), gender, & experience with the morphing problem are only recorded. All measures are implemented with full considerations of the anonymity of participants. We have designed the GUI for the human observer study to benchmark the single image morphing detection in this work.

Figure 4 shows the screenshot of the web portal used for the human observer's study. The GUI is designed to display two face images at a time such that one corresponds to the 2D face and another corresponds to the 3D face. Then, the human observer is prompted to independently decide these face images as either morph or bona fide. The human observers are provided with an option to rotate the 3D face in different directions to make their decision effectively. Further, the

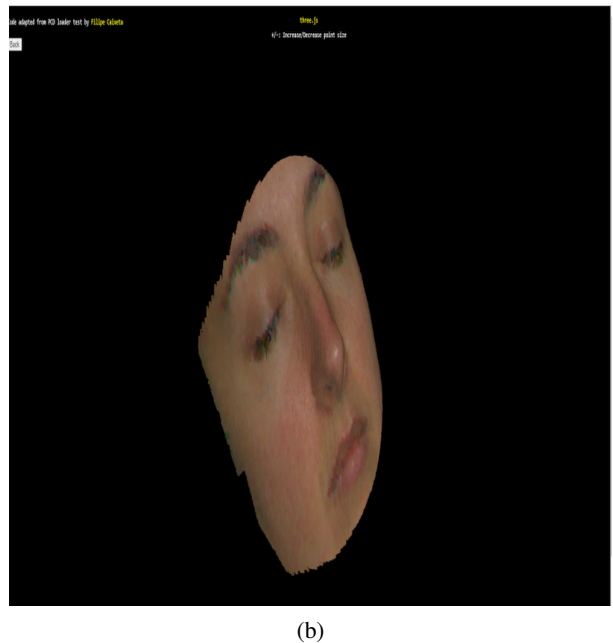
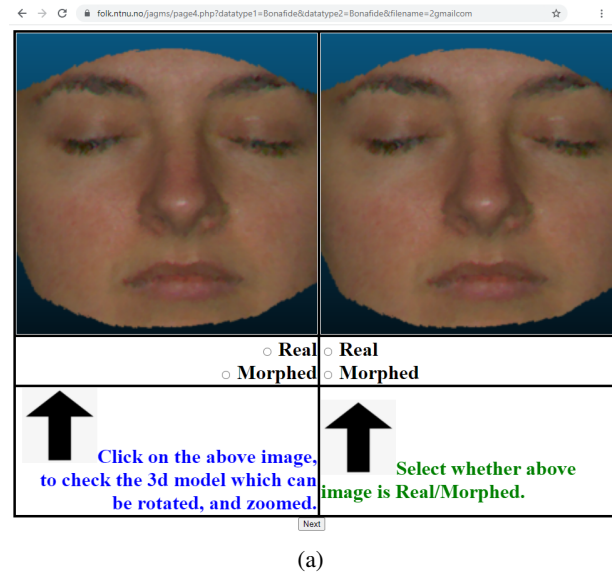


Fig. 4. Screenshots from the GUI of human observer web page (a) Full Page Screenshot, and (b) Screenshot of 3D model page.

opportunities to zoom in and zoom out the 3D face model are also provided. We have mainly selected to present both 2D/3D face images for human evaluation at the same time to check whether the 3D information might help detect the morphing attacks. Due to the time factor, we have used 19 bona fide and morph samples independently from 2D and 3D for human observer study. Thus, each human observer has spent around 20 minutes on average to complete this study. The detailed step-wise instructions on using the web portal are made available for every participant beforehand.

The human observer study is carried out using 36 different observers with and without face morphing experience. The quantitative results of the human observer study are shown in Figure 5. We summarize the human observers results from the

³<https://folk.ntnu.no/jagms>

Combined			Male		Female	
Algorithm	MMPMR%	FMMPR%	MMPMR%	FMMPR%	MMPMR%	FMMPR%
2D Vulnerability Analysis						
COTS	97.45%	89.78%	97.98%	90.65%	94.03%	86.36%
Arcface	63.81%	28.66%	64.92%	27.13%	59.70%	33.33%
3D Vulnerability Analysis						
LED3D [40]	81.69%	54.00%	82.67%	51.84%	77.61%	63.64%
PointNet++ [41]	95.65%	80.52%	95.32%	79.42%	95.52%	84.85%

TABLE II
VULNERABILITY ANALYSIS OF 2D AND 3D FRS

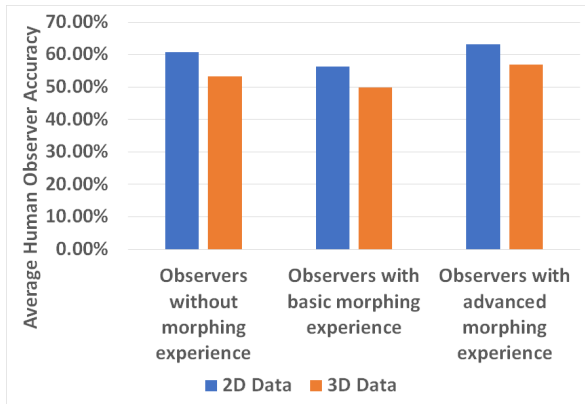


Fig. 5. Illustration of average accuracy of human observer study, note that 2D accuracy is always higher than 3D.

survey as follows:

- The average detection accuracy of human observers for 2D face bona fide samples is 55.83%, and 42.5% in a 3D face, respectively. The average detection accuracy of human observers for morphs in 2D is 58.33% and 51.85% in a 3D face. Thus, detection accuracy is similar for bona fide and morph in 2D. However, the detection accuracy in 3D is lower for bona fide when compared with morph.
- The average detection accuracy is similar for observers without morphing experience and basic morphing experience. Human observers with advanced morphing experience have the highest average detection accuracy. The observers without morphing experience perform similar to observers with basic morphing experience, which can be attributed to the innate human capacity to distinguish between bona fide v/s morphed.
- The survey further validates that generated 3D morphs are challenging to detect from human observations. The average detection accuracy of human observers does not exceed 63.15% which shows that 2D and 3D morphs generated in this work are high quality and difficult to detect.

The average detection accuracy in a 2D face is higher than that in a 3D face, which can be attributed to the following reasons:

- The fact that 2D morph is more prevalent, and thus observers generally look for specific artifacts in different

regions of the face makes the task relatively easy with a 2D face.

- The aspect of what artifacts to look at in 3D is unclear to the human observers, as they are not trained for this task.
- The quality of generated 3D morphs is high, so human observers find it difficult to distinguish the 3D morphs from the 3D bona fide.

C. Vulnerability Study

In this work, we benchmark the performance of the automatic FRS on both 2D and 3D face models. The 2D face vulnerability is computed using the color image and the 3D face vulnerability is computed based on depth-map/point cloud. We have used two different metrics to benchmark the vulnerability assessment that includes Mated Morphed Presentation Match Rate (MMPMR) [42] and Fully Mated Morphed Presentation Match Rate (FMMPMR) [43]. The vulnerability analysis is performed by enrolling the morphing image (2D/3D) and then obtaining the comparison score by probing both contributory data subjects' face images (2D/3D).

To compute the vulnerability of 2D face morphing images, we have used two different FRS such as Arcface [2] and a Commercial-off-the-Shelf (COTS) FRS ⁴. The 3D face vulnerability analysis is performed using Deep Learning-based FRS such as Led3D [40] and PointNet++ [41]. The thresholds for all FRS used in this work is set at FAR=0.1% following the guidelines of Frontex for border control [44]. The results are summarized in Table II, and the vulnerability plots are shown in Figure 6. Based on the obtained results, it can be noted that (1) Both 2D and 3D FRS are vulnerable to the generated face morphing attacks (2) Among the 2D FRS, the COTS indicates the highest vulnerability compared to the Arcface FRS. (3) Among the 3D FRS the PointNet++ [41] indicates the highest vulnerability. Thus, the quantitative results of the vulnerability analysis indicate the effectiveness of the generated 3D face morphing attacks.

D. Automatic 3D Face Point Cloud Quality Estimation

In this work, we estimate the visual quality based on the effectiveness of different types of features, including both color and geometry, as proposed in [45]. This study aims to

⁴The name of the COTS is not indicated to respect confidentiality

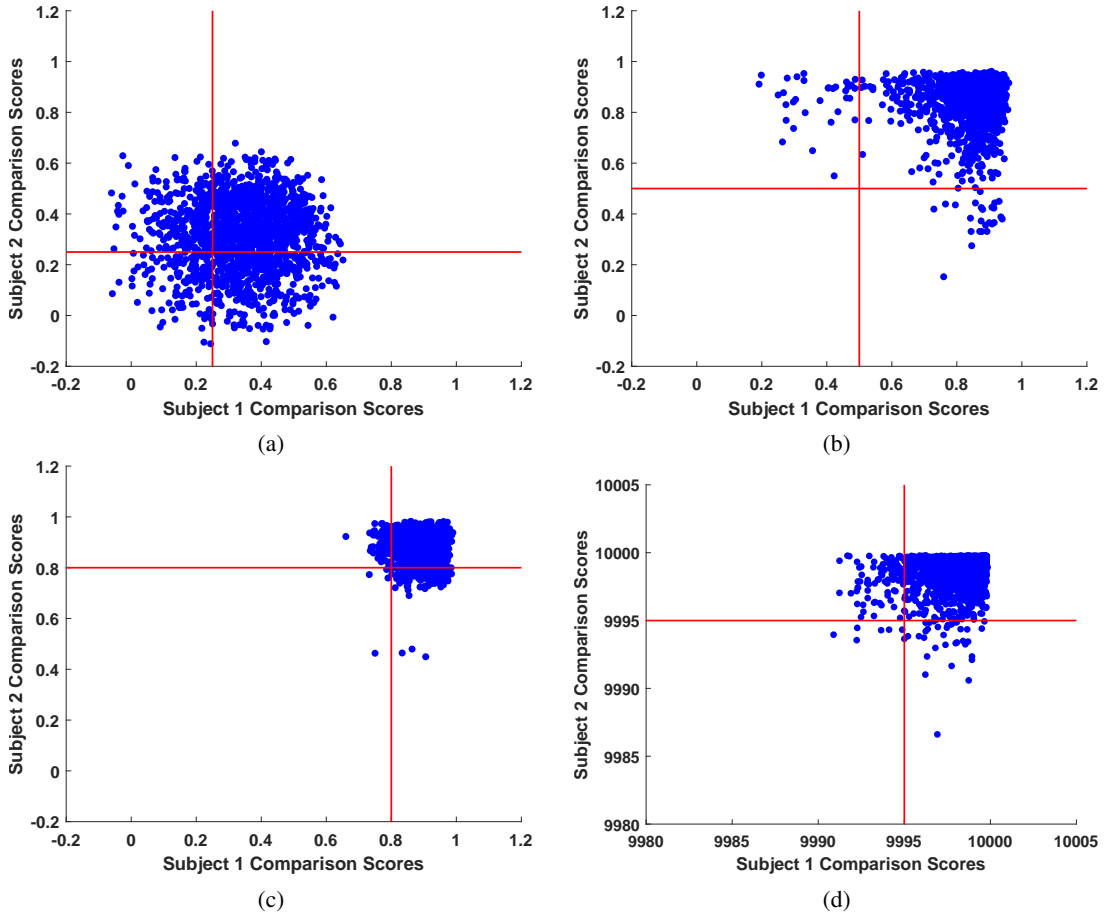


Fig. 6. Vulnerability Plots using 2D & 3D FRS. (a) 2D face FRS using Arcface [2], (b) 2D face FRS using COTS, and (c) 3D face FRS using Led3D [40], and (d) 3D face FRS using Pointnet++ [41] (Scaled by 10K times for visualization). Note COTS, PointNet++, and Led3D show high-level of vulnerability.

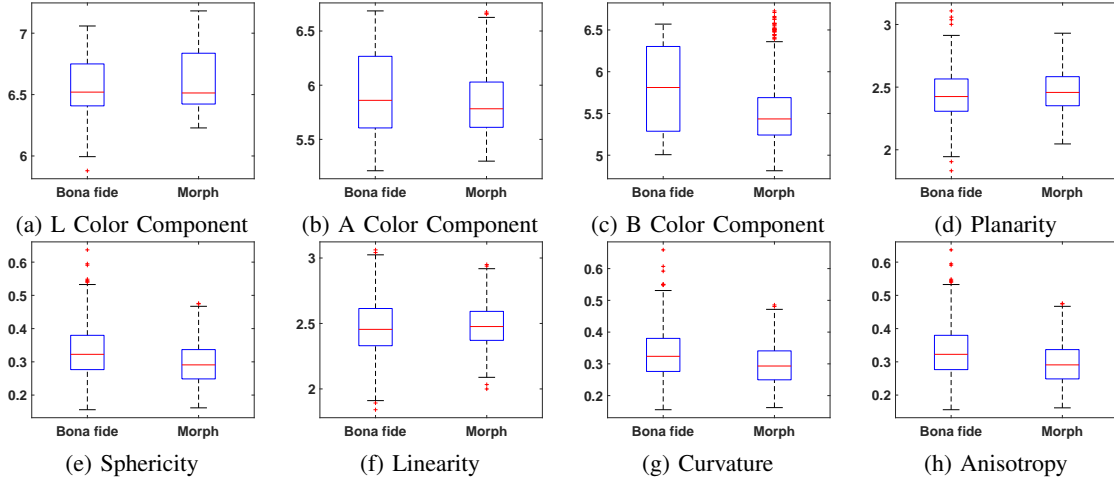


Fig. 7. Quality plots for 3D bona fide and morph based on color and geometry

quantitatively estimate the quality of the generated 3D face morphing point clouds and the bona fide 3D face point clouds to quantify the quality of the proposed morphing generation. To this extent, five different point cloud features based on geometry, namely curvature, anisotropy, linearity, planarity, sphericity, and three color information features, namely L color component, A color component, B color component, are computed to benchmark the quality based on the geometry of

the generated 3D morphing models.

Figure 7 shows the box plot of the eight different quality metrics for both 3D bona fide and 3D morphing point clouds. The quantitative values (mean and standard deviation) of different quality features are also shown in Table III. As noted from Figure 6, the quality estimations, mainly based on geometry, indicate the near-complete overlapping for 3D bona fide and 3D morph. Thus, the proposed 3D face morphing

3D Face Quality Features (mean \pm std. deviation)	Data type	
	Bona fide	Morphed
L Color	6.5614 \pm 0.2191	6.6076 \pm 0.2340
A Color	5.9368 \pm 0.3547	5.8546 \pm 0.3260
B Color	5.7998 \pm 0.5074	5.5326 \pm 0.4198
Linearity	2.4708 \pm 0.2196	2.4911 \pm 0.1776
Sphericity	0.3318 \pm 0.0807	0.2936 \pm 0.0592
Anisotropy	0.3318 \pm 0.0807	0.2936 \pm 0.0592
Curvature	0.3330 \pm 0.0821	0.2965 \pm 0.0606
Planarity	2.4430 \pm 0.2176	2.4711 \pm 0.1733

TABLE III
QUANTITATIVE VALUES OF QUALITY FEATURES FOR 3D FACE POINT CLOUDS CORRESPONDING TO 3D BONA FIDE AND MORPH BASED ON COLOR AND GEOMETRY

generation did not degrade the depth quality. Instead, it has achieved comparable quality based on geometry that of bona fide 3D models used for the morphing operation. Similar observation can also be noted with the color image quality estimation.

E. 3D Face Morphing Attack Detection

In this section, we present our proposed method for a single 3D model-based MAD. Because the 3D face morphing is extensively presented in this paper for the first time, there exists no state-of-the-art to detect these attacks. Therefore, we are motivated to develop 3D MAD techniques to detect these attacks reliably. The proposed 3D MAD techniques are based on the pre-trained 3D point-based networks that are used to extract the features as shown in Figure 8. Thus, given the 3D face point clouds, we first compute the features from the pre-trained network and in the next step, we feed the same to the linear support vector machine to make the final decision on either bona fide or morph. In this work, we have used three different pre-trained point cloud networks such as Pointnet [46], [47], Pointnet++ [41], [47] and SimpleView [47] independently to benchmark the 3D MAD performance. All three pre-trained CNNs are trained on ModelNet40 dataset [48].

The Pointnet [46], [47] is one of the earliest point-based classifications of deep learning networks invariant to the permutation of 3D vertices. Given the 3D face point clouds, we extract the feature from the classification task layer corresponding to the feature dimension of 4096. The Pointnet++ [41], [47] is the improved version of Pointnet [46], [47] achieved by introducing a hierarchical neural network that was applied recursively. In this work, given the 3D face point clouds, we extract the features from the classification task layer of the Pointnet++ to obtain a 40-dimensional feature vector. The SimpleView [47] network is based on projecting the point clouds to multiple view depth maps. In this work, given the 3D face point clouds, we extract the features from the classification task layer of the SimpleView network to obtain a 40-dimensional feature vector.

To effectively benchmark the performance of the proposed 3D MAD, we divide the newly collected dataset into two independent sets, namely training and testing. Training set consists of 3D bona fide and morphing samples from 21 unique data subjects and the testing set consists of 3D samples from

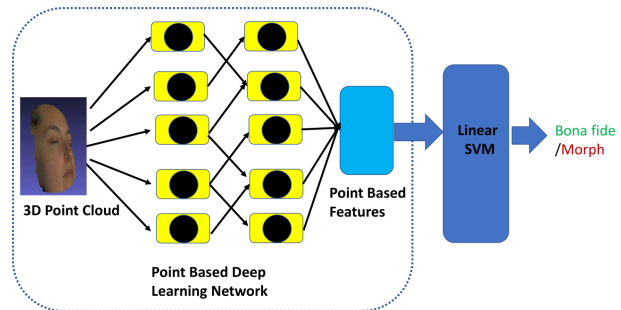


Fig. 8. Illustration of the Proposed 3D Morphing Attack Detection

20 unique data subjects. Thus, the training set consists of 168 bona fide and 194 morphed features and the testing set consists of 160 bona fide and 151 morphed features. Table IV shows the quantitative performance of the proposed 3D MAD techniques. Figure 9 shows the performance of individual algorithms in DET. The performance is benchmarked using ISO/IEC metrics [49] defined as Attack Presentation Classification Error Rate (APCER), which is the mis-classification rate of attack presentations and Bona fide Presentation Classification Error Rate (BPCER) is the mis-classification of bona fide presentation as attacks. Based on the obtained results, the best performance is obtained with the SimpleView [47] network with a D-EER of 1.59%.

Algorithm Proposed Method	D-EER (%)	BPCER @ APCER =	
		5%	10%
Pointnet [46]	2.57	3.12	2.5
Pointnet++ [41]	37.33	81.87	68.12
SimpleView [47]	1.59	2.5	0

TABLE IV
QUANTITATIVE PERFORMANCE OF THE PROPOSED 3D MAD TECHNIQUES

IV. DISCUSSION

Based on the extensive experiments and obtained results made above, the research questions formulated in Section I are answered as below.

- **RQ#1.** Does the proposed 3D face morphing generation technique yield a high-quality 3D morphed model?

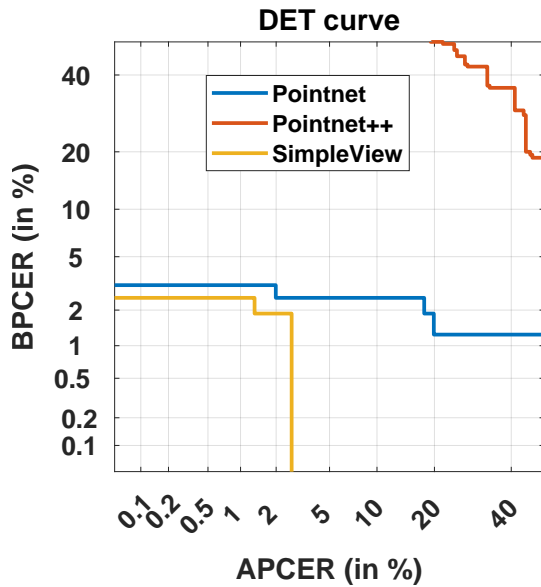


Fig. 9. DET Curve for the Proposed 3D Morphing Detection methods.

- Yes, the proposed method of generating the 3D face morphing has resulted in a high-quality morphed model almost similar to that of the original 3D bona fide. The quality analysis reported in Figure 7 and Table III also justifies the quality of the generated 3D morphs quantitatively as the quality values from 3D morphing show larger overlapping with the 3D bona fide. In addition, the human observer analysis reported in Section III-B also justifies the quality of the proposed 3D face morphing generation method as it is found reasonably difficult to detect based on the artefacts.
- **RQ#2.** Does the generated 3D face morphing model indicate the vulnerability for both automatic 3D FRS and human observers?
 - Yes, based on the analysis reported in the Section III-C the generated 3D face morphing model indicate a high degree of vulnerability for both automatic 3D FRS and human observers.
- **RQ#3.** Are the generated 3D face morphing models more vulnerable when compared to 2D face images for both automatic 3D FRS and human observers?
 - Equally vulnerable, the 3D face morphing models are more vulnerable than their 2D counterpart as shown in Figure 6 when using automatic FRS.
 - However, the vulnerability is almost comparable when evaluated by human observer study (see Section III-B) where one of the main reasons could be more prevalence of 2D morphs which makes human observers sensitive about which artifacts to look for.
- **RQ#4.** Can the 3D point cloud information be used to detect the 3D face morphing attacks reliably?
 - Yes, on using the proposed 3D face morphing attack Detection approaches (see Section III-E) the point cloud information can be used for reliable 3D morphing detection.

V. LIMITATIONS OF CURRENT WORK AND POTENTIAL FUTURE WORKS

Although the work presents a new dimension for face morphing attack generation and detection, especially in 3D, this work has few limitations. In the current scope of work, the 3D morph generation and detection are carried out on the high-quality 3D scans collected using the Artec Eva sensor. We have employed high-quality 3D face scans to achieve good enrolment quality scans that may reflect the real-life ID enrolment scenario. Thus, future works could investigate the proposed 3D morphing generation and detection techniques using low-quality (depth) 3D scans. Further, extending the study towards in-the-wild capture can also be considered in future work. As a second aspect, the analysis is carried out using 41 data subjects due to the present outbreak of the pandemic. However, future work can benchmark the proposed method on a large-scale dataset. As a third aspect, cleaning noise from 3D scans is tedious and sometimes requires manual intervention; thus, future work can develop a fully automated noise removal in 3D point clouds to easily the 3D morph generation.

VI. CONCLUSION

This work presented a new dimension for face morphing attacks generation and detection, especially in 3D. We have introduced a novel algorithm to generate high-quality 3D face morphing models using point clouds. To validate the attack potential of the newly generated 3D face morphing attacks, the vulnerability analysis is carried out using both 2D and 3D FRS. Further, the human observer analysis is also presented to investigate the usefulness of 3D information towards morph detection. Obtained results justify the high vulnerability of the proposed 3D face morphing models. We also presented an automatic quality analysis of the generated 3D morphing models that indicate a similar quality as the bona fide 3D scans. Finally, we have proposed three different 3D MAD algorithms to detect the 3D morphing attacks using pre-trained point-based CNN models. Extensive experiments indicate the efficacy of the proposed 3D MAD algorithms in detecting the 3D face morphing attacks.

ACKNOWLEDGMENT

This work is carried out under the partial funding of the Research Council of Norway (Grant No. IKTPLUSS 248030/O70).

REFERENCES

- [1] F. Schroff, D. Kalenichenko, and J. Philbin, "Facenet: A unified embedding for face recognition and clustering," in *Proceedings of the IEEE conference on computer vision and pattern recognition*, 2015, pp. 815–823.
- [2] J. Deng, J. Guo, N. Xue, and S. Zafeiriou, "Arcface: Additive angular margin loss for deep face recognition," in *Proceedings of the IEEE/CVF Conference on Computer Vision and Pattern Recognition*, 2019, pp. 4690–4699.
- [3] M. Ferrara, A. Franco, and D. Maltoni, "The magic passport," in *IEEE International Joint Conference on Biometrics*. IEEE, 2014, pp. 1–7.
- [4] R. Raghavendra, K. B. Raja, and C. Busch, "Detecting morphed face images," in *2016 IEEE 8th International Conference on Biometrics Theory, Applications and Systems (BTAS)*, 2016, pp. 1–7.

- [5] M. Ferrara, A. Franco, and D. Maltoni, "Face demorphing," *IEEE Transactions on Information Forensics and Security*, vol. 13, no. 4, pp. 1008–1017, 2017.
- [6] H. Zhang, S. Venkatesh, R. Ramachandra, K. Raja, N. Damer, and C. Busch, "Mipgan—generating strong and high quality morphing attacks using identity prior driven gan," *IEEE Transactions on Biometrics, Behavior, and Identity Science*, vol. 3, no. 3, pp. 365–383, 2021.
- [7] U. Scherhag, A. Nautsch, C. Rathgeb, M. Gomez-Barrero, R. N. Veldhuis, L. Spreeuwiers, M. Schils, D. Maltoni, P. Grother, S. Marcel *et al.*, "Biometric systems under morphing attacks: Assessment of morphing techniques and vulnerability reporting," in *2017 International Conference of the Biometrics Special Interest Group (BIOSIG)*. IEEE, 2017, pp. 1–7.
- [8] R. Raghavendra, K. Raja, S. Venkatesh, and C. Busch, "Face morphing versus face averaging: Vulnerability and detection," in *2017 IEEE International Joint Conference on Biometrics (IJCB)*. IEEE, 2017, pp. 555–563.
- [9] N. Damer, A. M. Saladie, A. Braun, and A. Kuijper, "Morgan: Recognition vulnerability and attack detectability of face morphing attacks created by generative adversarial network," in *2018 IEEE 9th International Conference on Biometrics Theory, Applications and Systems (BTAS)*. IEEE, 2018, pp. 1–10.
- [10] S. Venkatesh, H. Zhang, R. Ramachandra, K. Raja, N. Damer, and C. Busch, "Can gan generated morphs threaten face recognition systems equally as landmark based morphs?—vulnerability and detection," in *2020 8th International Workshop on Biometrics and Forensics (IWBF)*. IEEE, 2020, pp. 1–6.
- [11] S. Venkatesh, R. Ramachandra, K. Raja, and C. Busch, "Face morphing attack generation & detection: A comprehensive survey," *IEEE Transactions on Technology and Society*, 2021.
- [12] M. Ngan, P. Grother, K. Hanaoka, and J. Kuo, "Part 4: Morph - performance of automated face morph detection," https://pages.nist.gov/frvt/reports/morph/frvt_morph_report.pdf, 2021, [Online; accessed 16-October-2021].
- [13] A. A. Deeb, "Uae reviews features of new id card, 3d photo included," <https://www.gulftoday.ae/news/2021/08/05/uae-reviews-features-of-new-id-card-3d-photo-included>, 2020, [Online; accessed 16-October-2021].
- [14] IDEMIA, "Stereo laser image," <https://www.idemia.com/wp-content/uploads/2021/02/stereo-laser-image-idemia-brochure-202007.pdf>, 2020, [Online; accessed 18-October-2021].
- [15] J. W. J. ter Hennepe, "3d photo id," https://www.icao.int/Meetings/AMC/MRTD-SEMINAR-2010-AFRICA/Documentation/11_Morpho-3DPhotoID.pdf, 2010, [Online; accessed 16-October-2021].
- [16] D. Face Based ABC Systems, "3d face enrolment for id cards," http://cubox.aero/cubox/php/en_product01-2.php?product=1/, 2021, [Online; accessed 18-October-2021].
- [17] S. Dent, "Using a 3d render as a french id card 'photo'," <https://engt.co/3EiPnQv>, 2017, [Online; accessed 16-October-2021].
- [18] ICAO, "Machine readable travel documents. part 11: Security mechanisms for mrtids. technical report doc 9303," 2021.
- [19] ISO/IEC JTC1 SC37 Biometrics, "ISO/IEC 39794-5:2019 information technology — extensible biometric data interchange formats — part 5: Face image data," 2019.
- [20] "Apple Face ID," https://en.wikipedia.org/wiki/Face_ID, 2017.
- [21] B. Egger, W. A. Smith, A. Tewari, S. Wuhler, M. Zollhoefer, T. Beeler, F. Bernard, T. Bolkart, A. Kortylewski, S. Romdhani *et al.*, "3d morphable face models—past, present, and future," *ACM Transactions on Graphics (TOG)*, vol. 39, no. 5, pp. 1–38, 2020.
- [22] Y. Yao, B. Deng, W. Xu, and J. Zhang, "Quasi-newton solver for robust non-rigid registration," in *Proceedings of the IEEE/CVF Conference on Computer Vision and Pattern Recognition (CVPR)*, June 2020.
- [23] H. Li, R. W. Sumner, and M. Pauly, "Global correspondence optimization for non-rigid registration of depth scans," *Computer Graphics Forum (Proc. SGP'08)*, vol. 27, no. 5, July 2008.
- [24] N. Gelfand, N. J. Mitra, L. J. Guibas, and H. Pottmann, "Robust global registration," in *Symposium on Geometry Processing*, 2005, pp. 197–206.
- [25] P. J. Besl and N. D. McKay, "Method for registration of 3-d shapes," in *Sensor fusion IV: control paradigms and data structures*, vol. 1611. International Society for Optics and Photonics, 1992, pp. 586–606.
- [26] "Artec eva sensor," <https://bit.ly/3BiGnJ1>, 2021, [Online; accessed 16-October-2021].
- [27] P. Cignoni, M. Callieri, M. Corsini, M. Dellepiane, F. Ganovelli, and G. Ranzuglia, "MeshLab: an Open-Source Mesh Processing Tool," in *Eurographics Italian Chapter Conference*, V. Scarano, R. D. Chiara, and U. Erra, Eds. The Eurographics Association, 2008.
- [28] B. Gärtner, "Fast and robust smallest enclosing balls," in *European symposium on algorithms*. Springer, 1999, pp. 325–338.
- [29] D. Haehnel, S. Thrun, and W. Burgard, "An extension of the icp algorithm for modeling nonrigid objects with mobile robots," in *IJCAI*, vol. 3, 2003, pp. 915–920.
- [30] M. Kazhdan and H. Hoppe, "Screened poisson surface reconstruction," *ACM Transactions on Graphics (ToG)*, vol. 32, no. 3, pp. 1–13, 2013.
- [31] G. Guennebaud and M. Gross, "Algebraic point set surfaces," *ACM Trans. Graph.*, vol. 26, no. 3, p. 23–es, Jul. 2007. [Online]. Available: <https://doi.org/10.1145/1276377.1276406>
- [32] A. C. Öztireli, G. Guennebaud, and M. Gross, "Feature preserving point set surfaces based on non-linear kernel regression," in *Computer graphics forum*, vol. 28, no. 2. Wiley Online Library, 2009, pp. 493–501.
- [33] D. E. King, "Dlib-ml: A machine learning toolkit," *Journal of Machine Learning Research*, vol. 10, pp. 1755–1758, 2009.
- [34] A. Telea, "An image inpainting technique based on the fast marching method," *Journal of graphics tools*, vol. 9, no. 1, pp. 23–34, 2004.
- [35] E. Rublee, V. Rabaud, K. Konolige, and G. Bradski, "Orb: An efficient alternative to sift or surf," in *2011 International Conference on Computer Vision*, 2011, pp. 2564–2571.
- [36] J. D. Foley, A. Van Dam, S. K. Feiner, J. F. Hughes, and R. L. Phillips, *Introduction to computer graphics*. Addison-Wesley Reading, 1994, vol. 55.
- [37] P. Phillips, P. Flynn, T. Scruggs, K. Bowyer, J. Chang, K. Hoffman, J. Marques, J. Min, and W. Worek, "Overview of the face recognition grand challenge," in *2005 IEEE Computer Society Conference on Computer Vision and Pattern Recognition (CVPR'05)*, vol. 1, 2005, pp. 947–954 vol. 1.
- [38] L. Yin, X. Wei, Y. Sun, J. Wang, and M. J. Rosato, "A 3d facial expression database for facial behavior research," in *7th international conference on automatic face and gesture recognition (FGR06)*. IEEE, 2006, pp. 211–216.
- [39] T. Maurer, D. Guigonis, I. Maslov, B. Pesenti, A. Tsaregorodtsev, D. West, and G. Medioni, "Performance of geometrix activeid™ tm 3d face recognition engine on the frgc data," in *2005 IEEE Computer Society Conference on Computer Vision and Pattern Recognition (CVPR'05)-Workshops*. IEEE, 2005, pp. 154–154.
- [40] G. Mu, D. Huang, G. Hu, J. Sun, and Y. Wang, "Led3d: A lightweight and efficient deep approach to recognizing low-quality 3d faces," in *Proceedings of the IEEE/CVF Conference on Computer Vision and Pattern Recognition (CVPR)*, June 2019.
- [41] C. R. Qi, L. Yi, H. Su, and L. J. Guibas, "Pointnet++: Deep hierarchical feature learning on point sets in a metric space," *arXiv preprint arXiv:1706.02413*, 2017.
- [42] U. Scherhag, A. Nautsch, C. Rathgeb, M. Gomez-Barrero, R. N. J. Veldhuis, L. Spreeuwiers, M. Schils, D. Maltoni, P. Grother, S. Marcel, R. Breithaupt, R. Ramachandra, and C. Busch, "Biometric systems under morphing attacks: Assessment of morphing techniques and vulnerability reporting," in *2017 International Conference of the Biometrics Special Interest Group (BIOSIG)*, 2017, pp. 1–7.
- [43] S. Venkatesh, H. Zhang, R. Ramachandra, K. Raja, N. Damer, and C. Busch, "Can gan generated morphs threaten face recognition systems equally as landmark based morphs? - vulnerability and detection," in *2020 8th International Workshop on Biometrics and Forensics (IWBF)*, 2020, pp. 1–6.
- [44] FRONTEx, "Best practice technical guidelines for automated border control abc systems," 2015.
- [45] Z. Zhang, "No-reference quality assessment for 3d colored point cloud and mesh models," *arXiv preprint arXiv:2107.02041*, 2021.
- [46] C. R. Qi, H. Su, K. Mo, and L. J. Guibas, "Pointnet: Deep learning on point sets for 3d classification and segmentation," in *Proceedings of the IEEE conference on computer vision and pattern recognition*, 2017, pp. 652–660.
- [47] A. Goyal, H. Law, B. Liu, A. Newell, and J. Deng, "Revisiting point cloud shape classification with a simple and effective baseline," *International Conference on Machine Learning*, 2021.
- [48] Z. Wu, S. Song, A. Khosla, F. Yu, L. Zhang, X. Tang, and J. Xiao, "3d shapenets: A deep representation for volumetric shapes," in *Proceedings of the IEEE conference on computer vision and pattern recognition*, 2015, pp. 1912–1920.
- [49] ISO/IEC JTC1 SC37 Biometrics, "ISO/IEC IS 30107-3. information technology - biometric presentation attack detection - part 3: Testing and reporting," 2017.